Distribution Categories:
LMFBR—Safety: Base Technology (UC-79p)
LMFBR—Structural Materials and Design Engineering: Base Technology (UC-79h)

ANL-82-47

ANL--82-47

DE83 002321

ARGONNE NATIONAL LABORATORY
9700 South Cass Avenue
Argonne, Illinois 60439

A COUPLED HEAT-CONDUCTION AND THERMAL-STRESS FORMULATION USING EXPLICIT INTEGRATION

by

A. H. Marchertas and R. F. Kulak

Reactor Analysis and Safety Division

June 1982

TABLE OF CONTENTS

LIST OF FIGURES

A COUPLED HEAT CONDUCTION AND THERMAL STRESS FORMULATION USING EXPLICIT INTEGRATION

by

A. H. Marchertas
R. F. Kulak

ABSTRACT

The formulation needed for the conductance of heat by means of explicit integration is presented. The implementation of these expressions into a transient structural code, which is also based on explicit temporal integration, is described. Comparisons of theoretical results with code predictions are given both for one-dimensional and two-dimensional problems. The coupled thermal and structural solution of a concrete crucible, when subjected to a sudden temperature increase, shows the history of cracking. The extent of cracking is compared with experimental data.

I. INTRODUCTION

The first requirements of thermal stress analysis is an accurate description of the temperature distribution within the given structure. Thus the computation of temperatures is an essential part of a code intended for thermal stress analysis.

The explicit time integration scheme has been adopted in our codes for stress analysis of concrete under high temperatures. This has been primarily dictated by the highly non-linear concrete behavior and the relative ease of accounting for non-linearity in this type of programming. Although explicit time integration has been used mostly for transient problems, we found it also very convenient to use for static problems by incorporating the dynamic relaxation technique.

The procedure of determining the temperature field in the structure should be an integral part of a computer code designed for thermal stress analysis. Since currently available heat conduction calculation procedures are based on iterative-type procedures, we have developed our own explicit technique.

The objective of this report is to outline the formulation used in the thermal calculations and their implementation into the structural code. Furthermore, comparisons of theoretical and analytical solutions are shown which attest to the validity of the thermal conduction calculations. Example solutions are then given illustrating the coupled thermal and structural aspects of concrete cracking. The results show that the developed code can apply well to both transient and steady state problems.

The equations required for the explicit temperature calculations are derived for the axisymmetric quadrilateral four-node continuum element, which reduce to the corresponding plane element. The expressions are generalized for numerical calculations using the Gaussian integration procedure. Because we found from previous experience that one-point integration per element is usually sufficient in thermal calculations, the general expressions are simplified for this case and presented in the report. Stability of the thermal explicit solution is evaluated and the stability of the time step is presented.

Numerical results of transient and steady state problems are shown for several examples. These results are compared with known theoretical solutions. The theoretical and code-generated results are in very good agreement. The analytical results of a test crucible subjected to hot temperature are also compared with experimental data as far as the extent of cracking is concerned. The code results are shown to be in close correspondence to the test observations.

II. ANALYTICAL APPROACH

A. Finite-Element Equations

The transient heat conduction equation is given by

$$\rho c \frac{\partial T}{\partial t} = \nabla\cdot(k\nabla T) + Q \ , \tag{1}$$

in which ρ is the density, c is the specific heat, k is the thermal conductivity, t is the time, T is the temperature and Q is the internal heat source per unit volume. Following a Galerkin approach, the following finite element form for Eq. (1) is obtained

$$[C]\left\{\frac{\partial T}{\partial t}\right\} + [K]\{T\} = \frac{1}{\rho c}[C]\{Q\} + [B]\{\bar{n}\cdot\bar{q}\}\ , \tag{2}$$

where [C] is the capacitance matrix, [K] is the conductance matrix, [B] is the surface matrix, {T} a column matrix of nodal temperatures, {Q} a column matrix of nodal internal-heat source, $\bar{q}$ is the surface heat flux vector, and $\bar{n}$ is the surface normal. The following definitions are used for [C], [K] and [B] in terms of the element shape function:

$$[C_{ij}] = \rho c \int_V [\phi_i \phi_j] dV\ , \tag{3}$$

$$[K_{ij}] = k \int_V [\nabla\phi_i \cdot \nabla\phi_j] dV\ , \tag{4}$$

$$[B_{ij}] = \int_S [\phi_i \phi_j] dS\ , \tag{5}$$

where ϕ_i is the shape function and ρ, c, and k are assumed to be constant within an element.

Equation (2) is adapted here for quadrilateral continuum elements which will be used for modeling temperature variations in concrete structures. A diagram of the element chosen for this study is shown in Fig. 1 along with the local coordinate system (ξ, η). The following shape functions $\{\phi\}$ are used for the element:

$$\{\phi\} = \frac{1}{4}\begin{Bmatrix} (1-\xi)(1-\eta) \\ (1+\xi)(1-\eta) \\ (1+\xi)(1+\eta) \\ (1-\xi)(1+\eta) \end{Bmatrix}\ . \tag{6}$$

An explicit-type integration scheme for a finite element formulation of heat conduction was previously developed.[1] The modified expression for the governing equation in terms of the definitions in Eqs. (3) through (5) is as follows:

$$r_c = \frac{1}{4}(r_1 + r_2 + r_3 + r_4)$$

$$z_c = \frac{1}{4}(z_1 + z_2 + z_3 + z_4)$$

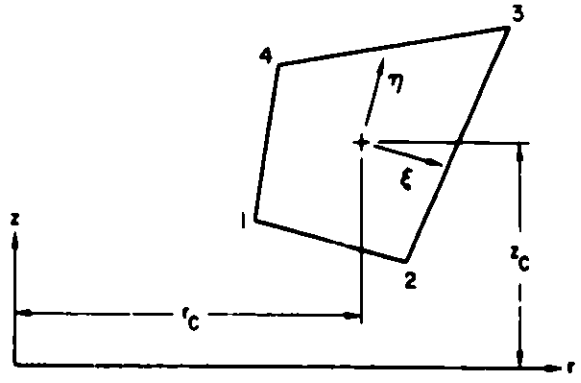

Fig. 1. Global and Local Coordinates of the Quadrilateral Element.

$$[C]\{T\}^{p+1} = [C]\{T\}^{p} - \Delta t\left([K]\{T\}^{p} - \frac{1}{\rho c}[C]\{Q\} - [B]\{\bar{n}\cdot\bar{q}\}\right) , \tag{7}$$

where Δt is the time step and p is the time step number. This is the form that we have adopted for our work.

B. Lumped Capacitance Matrix

The integrand function $[\phi_i \phi_j]$ of Eq. (3) is given in terms of the shape function; when the individual terms are evaluated for a rectangular element, the capacitance matrix becomes as follows:[1]

$$[C] = \frac{\rho c V}{36}\begin{bmatrix} 4 & 2 & 1 & 2 \\ 2 & 4 & 2 & 1 \\ 1 & 2 & 4 & 2 \\ 2 & 1 & 2 & 4 \end{bmatrix},$$

where V is the volume of the element. By assuming a lumped capacitance matrix we thus get

$$[C] = \frac{\rho c V}{4}\begin{bmatrix} 1 & 0 & 0 & 0 \\ 0 & 1 & 0 & 0 \\ 0 & 0 & 1 & 0 \\ 0 & 0 & 0 & 1 \end{bmatrix}, \tag{8}$$

where the total magnitude is equally divided to the four associated element nodes. It should be noted that the lumped capacitance matrix is equivalent to the structural mass matrix when multiplied by the constant specific heat, c, i.e.,

$$[C] = c\,[m] , \tag{9}$$

where $[m]$ is the lumped mass matrix as used in the structural codes with explicit integration schemes. The incorporation of the capacitance matrix into a structural code becomes, therefore, self explanatory.

C. Conductance Matrix

The conductance matrix [K] for an arbitrary quadrilateral element is to be evaluated numerically; thus, the volume of the element for cylindrical coordinates is $dV = r\, dr\, dz$.* Converting to local coordinates, we have

$$dV = r\, dr\, dz = |J| r\, d\xi\, d\eta ,$$

where ξ and η are the local coordinates and $|J|$ is the Jacobian and the constant 2π has been dropped from the expression. The conductance matrix of Eq. (4) in terms of the local coordinates then becomes

$$[K] = kr \int_{-1}^{1} \int_{-1}^{1} [B]^T [B] |J|\, d\xi\, d\eta . \tag{10}$$

An approximate value of the integral in Eq. (10) is obtained by the Gaussian integration; i.e., by finding the summation of the values of the function at a number of points multiplied by a weighting function at each point. For the integral in Eq. (10) we thus have

$$[K] \simeq kr \sum_{i=1}^{m} \sum_{j=1}^{n} [B(\xi_i, \eta_j)]^T [B(\xi_i, \eta_j)] |J(\xi_i, \eta_j)| W_i W_j , \tag{11}$$

where m and n are the number of integration points in the two coordinate directions ξ and η, and W_i and W_j are the corresponding weights. The coefficients of [B] were derived before[2] and are given as follows:

---

* It should be noted that the constant 2π is absent here and also in the mass matrix [m] of Eq. (9). This constant will also be deleted from all the individual terms of the heat conduction expression of Eq. (7). The advantage of doing it is that the same expression then holds also for the plane geometry, provided the axisymmetric parameter r assumes the meaning of width in the case of the plane geometry.

$$
\begin{aligned}
B_{11} &= \frac{1}{8|J|}\,(z_{24} - z_{34}\xi - z_{23}\eta)\,, \\
B_{12} &= \frac{1}{8|J|}\,(-z_{13} + z_{34}\xi + z_{14}\eta)\,, \\
B_{13} &= \frac{1}{8|J|}\,(-z_{24} + z_{12}\xi - z_{14}\eta)\,, \\
B_{14} &= \frac{1}{8|J|}\,(z_{13} - z_{12}\xi + z_{23}\eta)\,, \\
B_{21} &= \frac{1}{8|J|}\,(-r_{24} + r_{34}\xi + r_{23}\eta)\,, \\
B_{22} &= \frac{1}{8|J|}\,(r_{13} - r_{34}\xi - r_{14}\eta)\,, \\
B_{23} &= \frac{1}{8|J|}\,(r_{24} - r_{12}\xi + r_{14}\eta)\,, \\
B_{24} &= \frac{1}{8|J|}\,(-r_{13} + r_{12}\xi - r_{23}\eta)\,,
\end{aligned}
\tag{12}
$$

$$
\begin{aligned}
|J| = \frac{1}{8}\,[&(r_{13}z_{24} - r_{24}z_{13}) + \xi(r_{34}z_{12} - r_{12}z_{34}) \\
&+ \eta(r_{23}z_{14} - r_{14}z_{23})]\,,
\end{aligned}
\tag{13}
$$

where $r_{ij} = r_i - r_j$ and $z_{ij} = z_i - z_j$. If we introduce a new matrix for the matrix multiplication as $[D] = [B]^T[B]$, we find that these coefficients become:

$$
\begin{aligned}
D_{11} &= B_{11}B_{11} + B_{21}B_{21} , \\
D_{12} &= B_{11}B_{12} + B_{21}B_{22} , \\
D_{13} &= B_{11}B_{13} + B_{21}B_{23} , \\
D_{14} &= B_{11}B_{14} + B_{21}B_{24} , \\
D_{22} &= B_{12}B_{12} + B_{22}B_{22} , \\
D_{23} &= B_{12}B_{13} + B_{22}B_{23} , \\
D_{24} &= B_{12}B_{14} + B_{22}B_{24} , \\
D_{33} &= B_{13}B_{13} + B_{23}B_{23} , \\
D_{34} &= B_{13}B_{14} + B_{23}B_{24} , \\
D_{44} &= B_{14}B_{14} + B_{24}B_{24} ,
\end{aligned}
\tag{14}
$$

and due to symmetry,

$$
D_{21} = D_{12}, \qquad D_{41} = D_{14},
$$

$$
D_{31} = D_{13}, \qquad D_{42} = D_{24},
$$

$$
D_{32} = D_{23}, \qquad D_{43} = D_{34},
$$

In many applications only one integration per element is required. This simplifies the above expressions considerably, because then $\xi = \eta = 0$. For this case the components of the [D] matrix of Eqs. (14) become

$$D_{11} = \frac{1}{64|J|^2}\left(r_{24}r_{24} + z_{24}z_{24}\right) = -D_{13} = -D_{31} = D_{33} ,$$

$$D_{12} = -\frac{1}{64|J|^2}\left(r_{13}r_{24} + z_{13}z_{24}\right) = -D_{14} = D_{21} = -D_{23} = -D_{32} = D_{34} = -D_{41} = D_{43} , \tag{15}$$

$$D_{22} = \frac{1}{64|J|^2}\left(r_{13}r_{13} + z_{13}z_{13}\right) = -D_{24} = -D_{42} = D_{44} ,$$

and $|J| = \frac{1}{8}\left(r_{13}z_{24} - r_{24}z_{13}\right)$.

The matrix multiplication of conductance and temperature as needed in Eq. (7) for this case becomes

$$[K]\{T_i\} = 4kr|J|\ \{F_i\} , \tag{16}$$

where

$$\begin{aligned} F_1 &= D_{11}(T_1 - T_3) + D_{12}(T_2 - T_4) , \\ F_2 &= D_{12}(T_1 - T_3) + D_{22}(T_2 - T_4) , \\ F_3 &= -F_1 , \\ F_4 &= -F_2 . \end{aligned} \tag{17}$$

For the quadrilateral element the average radius r can be approximated by

$$r = \frac{1}{4}\left(r_1 + r_2 + r_3 + r_4\right) . \tag{18}$$

The same formulation also applies to a plane quadrilateral element, except then r takes the meaning of width of the plane element.

D. Surface Heat Flux Matrix

The surface heat flux may also be expressed in terms of element variables similar as has been done in the case of the conductance matrix. It is much more efficient numerically, however, to regard the surface heat flux as a boundary phenomenon and treat it the same way as pressure is generally accounted for in structural codes.

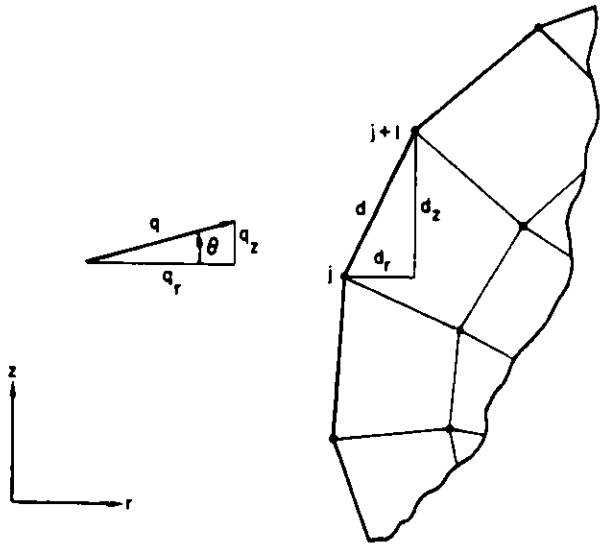

Fig. 2. Flux Applied at the Boundary of the Model.

In Fig. 2 the flux vector q is shown to act at an angle θ counter-clockwise from the r-axis. As it impinges on a distance |d| of two successive boundary nodes, j and j+1, the length of the flux normal to the surface becomes $|q_r d_z - q_z d_r|/|d|$ where $q_r = q\cos\theta$ and $q_z = q\sin\theta$. The effective flux on the surface area $r|d|$ is equally subdivided to the two nodes j and j+1 and become

$$q_j = q_{j+1} = \frac{r}{2}\left|q_r d_z - q_z d_r\right| , \tag{19}$$

where

$$r = \frac{1}{2}\left(r_j + r_{j+1}\right) .$$

Note that this same expression also holds for the plane boundary, except r is then substituted by the width of the plane element.

III. SUMMARY OF THERMAL CALCULATIONS

If the lumped capacitance matrix of Eq. (9) is substituted by the mass matrix in Eq. (7) and the flux term separated, we have

$$\{T\}^{p+1} = \{T\}^{p} - \frac{\Delta t}{c}\,[m]^{-1}\left([K]\{T\}^{p} - \{f\}^{p}\right), \tag{20}$$

where

$$\{f\}^p = \frac{1}{\rho}[m]\{Q\}^p + [B]\{\underset{\sim}{n}\cdot\underset{\sim}{q}\}^p \ . \tag{21}$$

Equation (20) provides the means of calculating the nodal temperatures in an explicit manner. Once the nodal temperatures are known, the temperature at any point in the element can be interpolated in terms of the four nodal point values $\{T\}$ as

$$T = \{\phi\}^T\{T\} \ . \tag{22}$$

Equation (20) can thus be coupled with the structural calculation so that the temperature is updated in the same way as the displacements, velocities and accelerations are in the structural code. The stability of Eq. (20), which provides a guide for the maximum Δt, is considered in Section IV.

IV. STABILITY OF THERMAL SOLUTION

A. System Eigenvalue Approach

The aim in the numerical integration of the heat conduction equations is to obtain a good approximation to the thermal response of the structure. The numerical integration is successful if it is stable and accurate. Here we used an explicit-type of temporal integrator, and it is known that explicit integrators become unstable when the calculational time step Δt_c, exceeds the critical time step, Δt_{cr} (i.e., the stability limit). In contrast, the accuracy of an explicit computation is not of concern because the computational time step is, usually by necessity, small enough to accurately integrate the system equations. In this section, we perform a stability analysis and present methods for estimating the stability limit.

The associated eigenproblem for Eq. (2) expressed in the basis of thermal mode vectors is given by

$$([K] - \lambda^i[C])\{X^i\} = \{0\} \ , \tag{23}$$

where λ^i is the ith eigenvalue or thermal frequency of the discretized system and $\{X^i\}$ the corresponding mode vector. We transform our equilibrium equations by applying the following transformation to the nodal temperatures

$$\{T\} = [P]\{\theta\} , \tag{24}$$

where $[P]$ is the modal matrix whose columns are the eigenvectors and $\{\theta\}$ is a generalized temperature vector. Using the above transformation and appropriate orthogonality conditions, the thermal equilibrium equations are recast in the following form

$$\{\dot{\theta}\} + [\Lambda]\{\theta\} = [P]^T\{R\} = \{\tilde{R}\} , \tag{25}$$

where $[\Lambda]$ is a diagonal matrix of the eigenvalues and $\{R\}$ is the right-hand side of Eq. (2). It should be noted that Eq. (25) represents a set of NDOF uncoupled equations where NDOF is the number of degrees of freedom of the discretized model. A typical equation from Eq. (25) may be written as

$$\dot{\theta} + \lambda\theta = \tilde{R} \tag{26}$$

To numerically integrate Eq. (26) we used the forward difference formulation

$$\frac{d\theta(t)}{dt} = \frac{\theta(t + \Delta t) - \theta(t)}{\Delta t} \tag{27}$$

to obtain the following difference equation for updating the temperature by one time step

$$\theta(t + \Delta t) = (1 - \lambda\Delta t)\ \theta(t) + \tilde{R}(t)\ \Delta t . \tag{28}$$

To investigate the stability of this recursion relation we study the solution after n time-steps for the case of zero thermal load. The solution is

$$\theta(t + n\Delta t) = (1 - \lambda\Delta t)^n\ \theta(t). \tag{29}$$

To assure that $\theta(t + n\Delta t)$ remains bounded as n increases, Δt must satisfy the relation

$$|1 - \lambda\Delta t| < 1 \tag{30}$$

and this is achieved if

$$\Delta t < \frac{2}{\lambda} . \tag{31}$$

The critical time step is obtained when the largest eigenvalue is used in Eq. (31).

B. Element Eigenvalue Approach

With the above approach, it is necessary to form the conductance and capacitance matrices for the assembled finite element model and then solve the eigenproblem [Eq. (23)]. This has the following drawbacks: (1) the assembly of the matrices is time consuming, (2) the matrices can require a large amount of core storage, and (3) the solution of a large eigenproblem can be time consuming. For these reasons we use an alternate approach to estimate the computational time-step. Hughes et al.[3] have shown that the maximum eigenvalue of the mesh is bounded by the largest of the element eigenvalues when the element is considered unassembled and unloaded, that is

$$\lambda_{max} < \max_{e} \left(\lambda^{e}_{max}\right) , \tag{32}$$

where λ^{e}_{max} is the maximum eigenvalue of each element. Our task now changes from that of finding the eigenvalues of the entire system to that of finding the eigenvalues of each element in the system. Furthermore, when the model is composed of identical elements or it is obvious which element has the largest eigenvalue, all that is required is to compute the eigenvalues for a single element. The provision has been incorporated into the code to compute the eigenvalues of selected elements. Thus, the user can make an initial run to obtain the critical time step for use in subsequent computational runs.

C. Equivalent One-Dimensional Element Approach

Another approach that can be used to estimate the critical time step is to compute the largest eigenvalue of an equivalent two node, one-dimensional

element. For this element the capacitance and conductance matrices are respectively given by

$$[C] = \frac{\rho c A L_{eq}}{2} \begin{bmatrix} 1 & 0 \\ 0 & 1 \end{bmatrix}, \tag{33}$$

$$[K] = \frac{kA}{L_{eq}} \begin{bmatrix} 1 & -1 \\ -1 & 1 \end{bmatrix}. \tag{34}$$

When the highest thermal mode eigenvector, which is given by

$$\{T\}^T = \begin{bmatrix} 1 & -1 \end{bmatrix}, \tag{35}$$

is used in the Rayleigh quotient we obtain the following estimate for the eigenvalue

$$\lambda = \frac{4k}{\rho c L_{eq}^2}, \tag{36}$$

where L_{eq} is taken to be the shortest distance between the nodes of the quadrilateral. An estimate for the critical time step is given by

$$\Delta t_{cr} = \frac{\rho c L_{eq}^2}{2k}. \tag{37}$$

Sample problem A of Section VI has shown that Eq. (37) provides a good estimate.

V. TIME PARAMETER USED IN STRUCTURAL COMPUTATIONS

When the explicit integration technique is applied to solve a transient problem, the time parameter used there pertains to the actual time of the physcial process. In quasi-steady state and steady state problems the time parameter in explicit integration loses its original meaning; it does not necessarily mean time, but rather becomes an ordinary integration parameter.

In fact, the explicit integration procedure when applied to steady-state problems is usually referred to as the dynamic relaxation technique.

In all explicit integration procedures the maximum time step is limited by the stability criterion of the structural problem. The duration of a given solution, for sake of efficiency, should then be as short as possible. In other than transient problems this can be accomplished by adjusting the "time" parameter used in the explicit integration; the real time of the problem can be reduced to the solution time. The extent of this reduction is limited on the other hand to a duration of time such that no inertial effects are introduced where none exist.

The dynamics of a given problem can be estimated by the first mode of vibration of the structure under consideration. The derivation of the reduction factor used is schematically illustrated in Fig. 3. The maximum rate of temperature increase at the surface is used to estimate an effective highest frequency of oscillation -- from which the period is calculated. The duration of the solution is made about five times larger than the period of the first mode of vibration. Note that the reduction factor calculated in this way must also be used to increase the diffusivity in the same proportion.

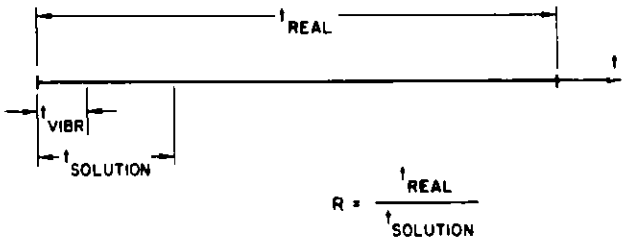

Fig. 3. Adjusting the Time Parameter for Explicit Integration.

VI. SAMPLE SOLUTIONS

The approximation involved in assuming a lumped capacitance matrix [C] is evaluated here by comparing the analytical code results with some known theoretical solutions. First comparisons are made of simple one-dimensional and two-dimensional problems. Finally, the thermal calculations are coupled with structural calculations to yield a cracking history of a concrete crucible into which liquid sodium is suddenly dumped.

A. Transient Response of a Semi-Infinite Solid

The problem considered here represents a semi-infinite solid which is subjected to a sudden heat flux applied on the surface. The analytical solution may be simulated by a one-dimensional model. Here we use quadrilateral elements (with one Gaussian integration per element) spanning a 3 cm distance into the solid, the cross-section of which is one square cm. In the

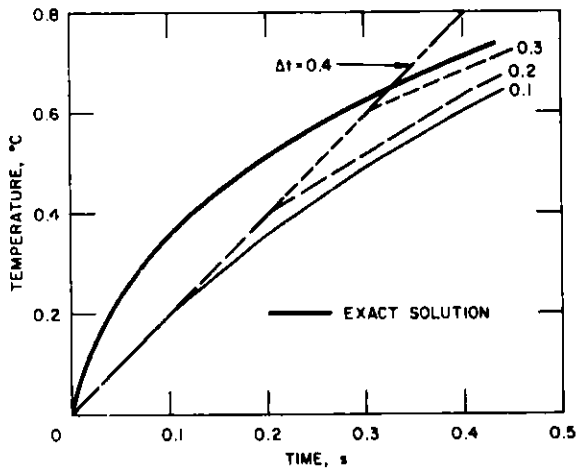

Fig. 4. Surface Temperature Simulation Using a Three-Element Model.

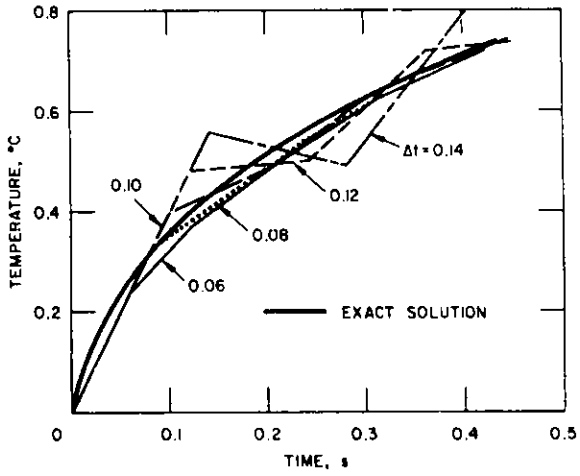

Fig. 5. Surface Temperature Simulation Using a Six Element Model.

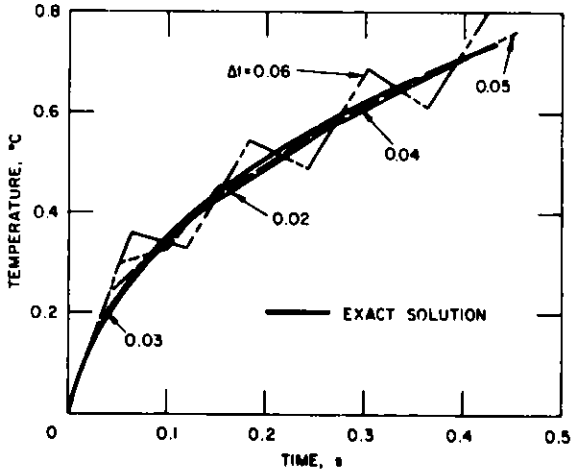

Fig. 6. Surface Temperature Simulation Using a Nine-Element Model.

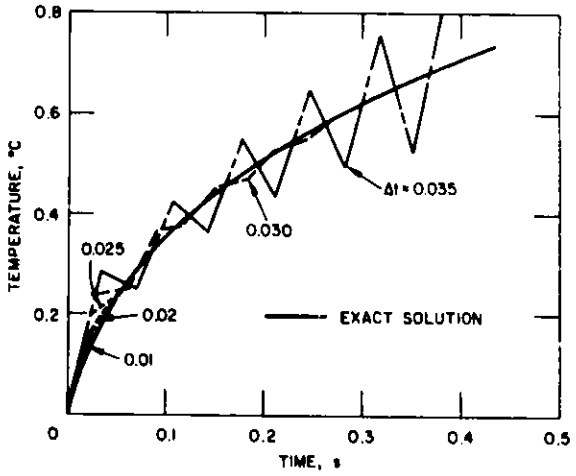

Fig. 7. Surface Temperature Simulation Using a 12-Element Model.

example we take thermal conductance k of 1 J/cm·s·°C, thermal capacity c as 1 J/kg·°C, mass density ρ of 1 kg/cm^3, and a unit heat flux per unit area. A series of solutions were obtained using different size elements. All of these runs are given in Figs. 4 through 8, which show the analytical and theoretical results of surface temperature history using different element sizes. These solutions provide a good check on the critical Δt as predicted by the stability criterion (Eq. 37). They also show that reasonable analytical results are obtained using even only a very small number of elements.

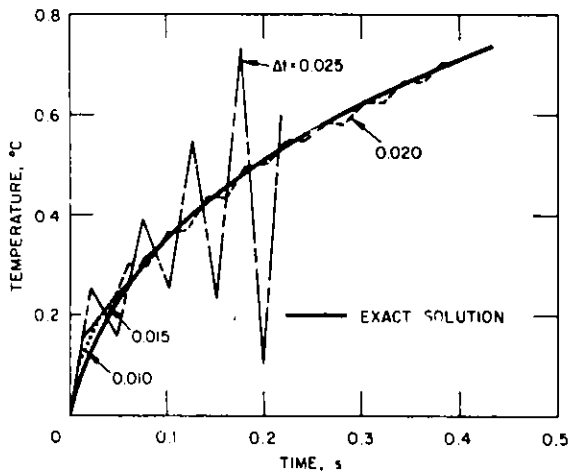

Fig. 8. Surface Temperature Simulation Using a 15-Element Model.

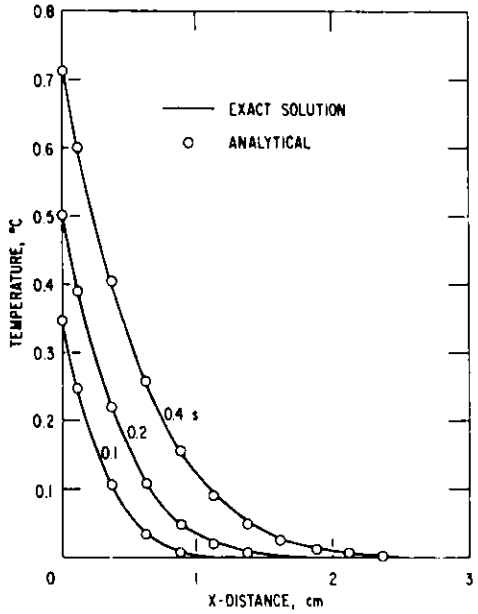

Fig. 9. Temperature Distributions in a Semi-infinite Solid.

For example, the 12 element analytical results using time increments Δt of 0.01, 0.02, 0.25, 0.30, and 0.35 s are shown in Fig. 7. It is observed that with Δt = 0.35 s the solution is unstable, while with Δt = 0.30 s it is still stable. At lower time steps deviations from the theoretical results occur at the beginning of the solution (during the first two or three time steps). Subsequent time steps yield analytical results very close to the theoretical values. This agreement is further illustrated in Fig. 9 which gives the temperature profiles within the body at different times for the 12-element model. The agreement of the theoretical and analytical results is very good.

B. Two-Dimensional Steady State Solution

The analytical results for a two-dimensional temperature field can be tested with the theoretical solution of a rectangular plate problem. Here, a sinusoidal temperature distribution is prescribed at one side, and zero temperature on the remaining sides. The theoretical steady-state temperature distribution along the line of symmetry is shown in Fig. 10. This figure also shows the analytical result, where the model uses one-half of the plate area. Four meshes were used to model this problem: 2 x 4 elements, 3 x 6 elements, 4 x 8 elements and 5 x 10 elements. A plot of contour isotherms for the four models are shown in Fig. 11. The case of 2 x 4 elements in the analytical model provides maximum deviation from the theoretical predictions, and the finer mesh models provide closer agreement. The overall agreement, however, appears very good.

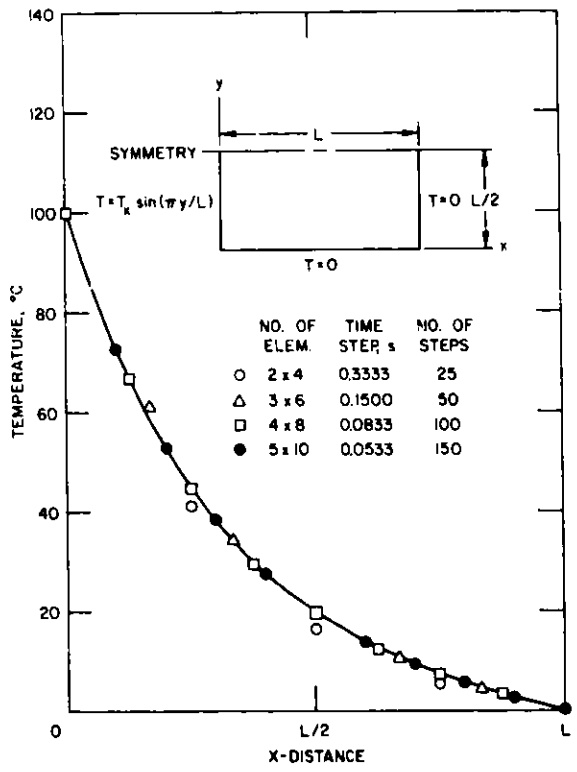

Fig. 10. Temperature Variation Along the Line of Symmetry.

C. A Coupled Solution of a Concrete Test Crucible

The analysis here pertains to a basalt concrete crucible for which experiment results are available.[4] Dimensions of the test crucible are shown in Fig. 12.[5] Liquid sodium of 600°C was dumped into the base cavity of the crucible resulting in a 13.2 cm deep pool. Measurements of temperature through the depth of the concrete slab were recorded and are reproduced in Fig. 13 indicating the temperature histories at different depths from the initial sodium-concrete interface. Posttest examination revealed an average surface erosion of approximately 5 cm deep in the crucible, as shown in Fig. 12. Furthermore, all the sodium had reacted with concrete leaving a cinder-like bed of reaction products. The cracking pattern of the crucible after the test is shown in

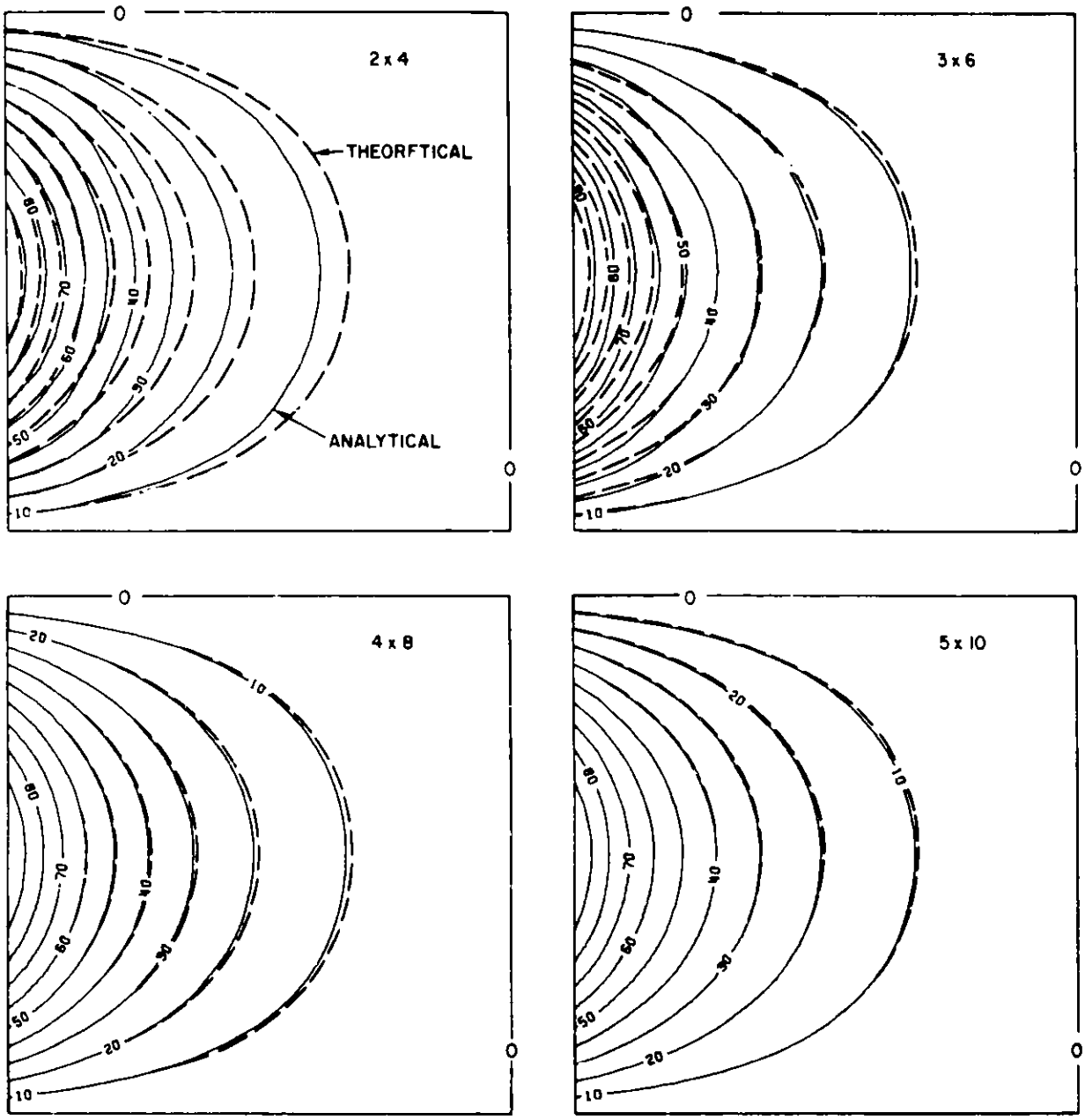

Fig. 11. Contour Plots of Temperature Distribution.

Fig. 14. It was also observed after this test that sodium had preferentially attacked the concrete along the cracks.

1. Analytical Model.

The crucible model discretization, as used in the analysis, is given in Fig. 15. Quadrilateral velocity-strain continuum elements were utilized with four Gaussian integration points per element. This model possesses a certain unusual feature in the use of the four-point quadrilateral elements

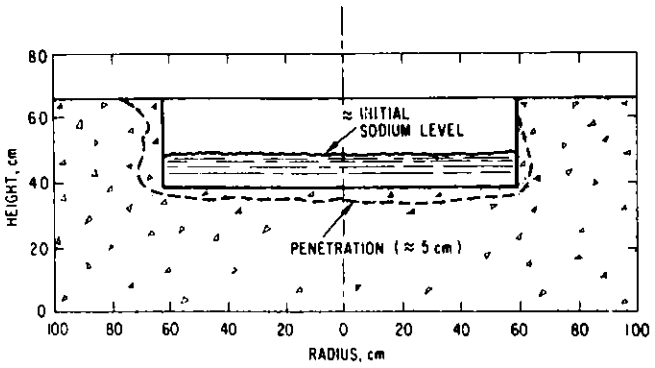

Fig. 12. Test Crucible Configuration. (Courtesy of SANDIA National Laboratories).

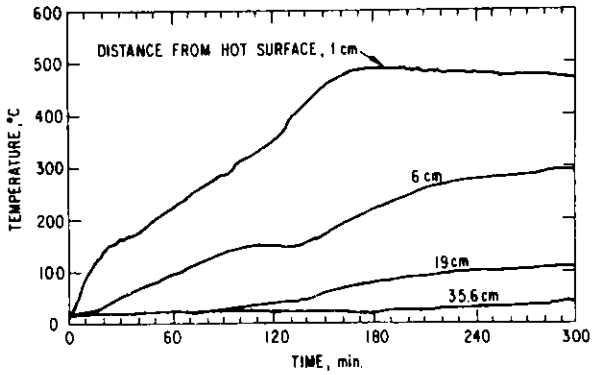

Fig. 13. Measured Crucible Temperatures. (Courtesy of SANDIA National Laboratories.)

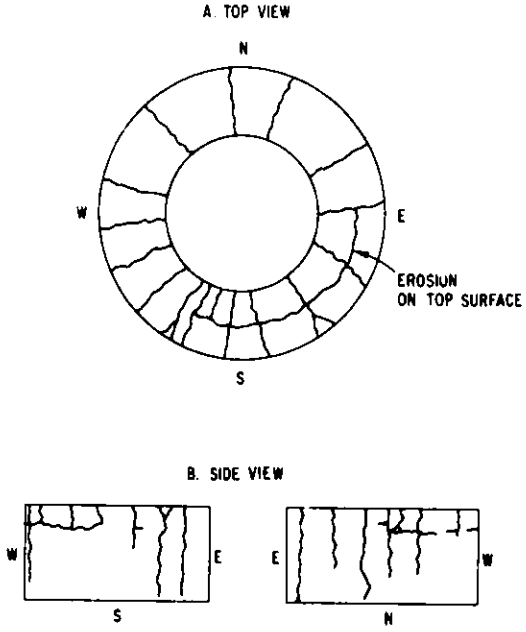

Fig. 14. Crucible Cracking Pattern. (Courtesy of SANDIA National Laboratories.)

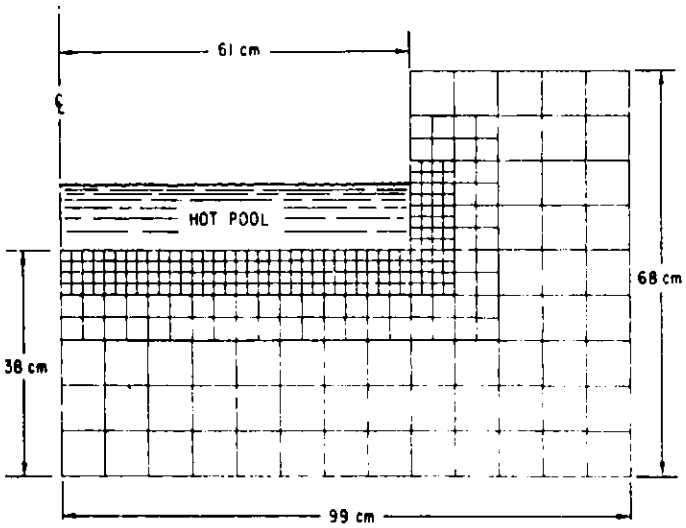

Fig. 15. Analytical Model.

requiring some explanation. The joining of smaller-size elements with larger-size elements here results in some nodes of the smaller elements to be positioned on the mid-sides of the larger elements. In order to make such a discretization of elements work, we have modified the standard solution procedure for this example as follows. The resulting internal forces and the flux contribution from thermal effects at the mid-side nodes are divided

equally between the two adjoining nodes. In addition, the accelerations of these nodes are assumed to be the average accelerations of the respective two adjoining nodes.

The time scale of the temperature history shown in Fig. 13 was increased by a factor 6 x 10^5 for calculational purposes. Consequently, with the time step of 5 μs, 6,000 increments were required to reach the 300 min. temperature conditions on the actual time scale. The dynamic relaxation technique, involving a mass-proportional damping of 3%, was used.

Figure 16 gives the stress-strain relations of concrete in compression at different temperatures.[6] A bilinear approximation is used for each temperature in which a linear elastic response was assumed up to the maximum stress, followed by a purely plastic resonse. The tensile limit was taken to be 0.1 of the corresponding compressive limit for each temperature. In addition, the stress beyond the tensile limit was reduced to zero linearly after a strain of 0.0005 m/m. A Poisson's ratio of 0.15 was assumed. The cracking model used is based on the maximum principal stress criterion and is described elsewhere.[7,8]

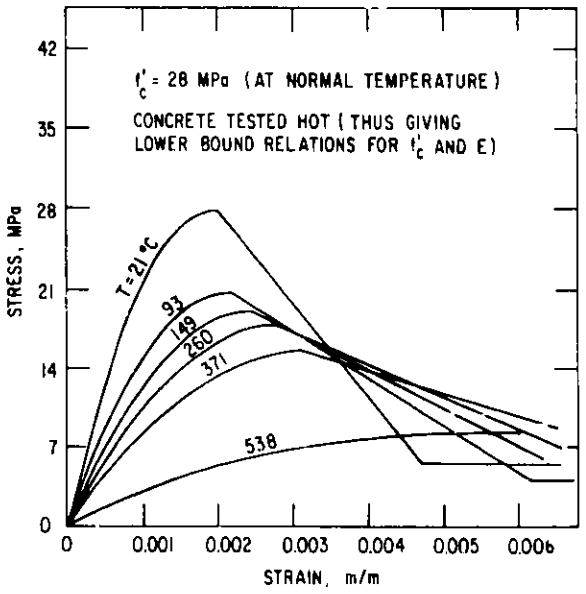

Fig. 16. Basalt Concrete Stress-Strain Compression Curves.

For thermal analysis the density of concrete was assumed to be 2.326 g/cm^3, effective specific heat was 0.929 J/g°C and thermal conductivity was 0.0182 J/cm s °C. These properties were assumed to be constant through the entire range of temperatures. Temperature calculations involve only one integration point per element [m = n = 1 in Eq. (22)].

The imposed temperature on the initial surface of the sodium-concrete interface was taken to be the same as the experimentally recorded temperature 1 cm deep from the surface (see Fig. 13). During the test the surface is eroded, and the 1 cm deep temperature data seems to be a reasonable value to

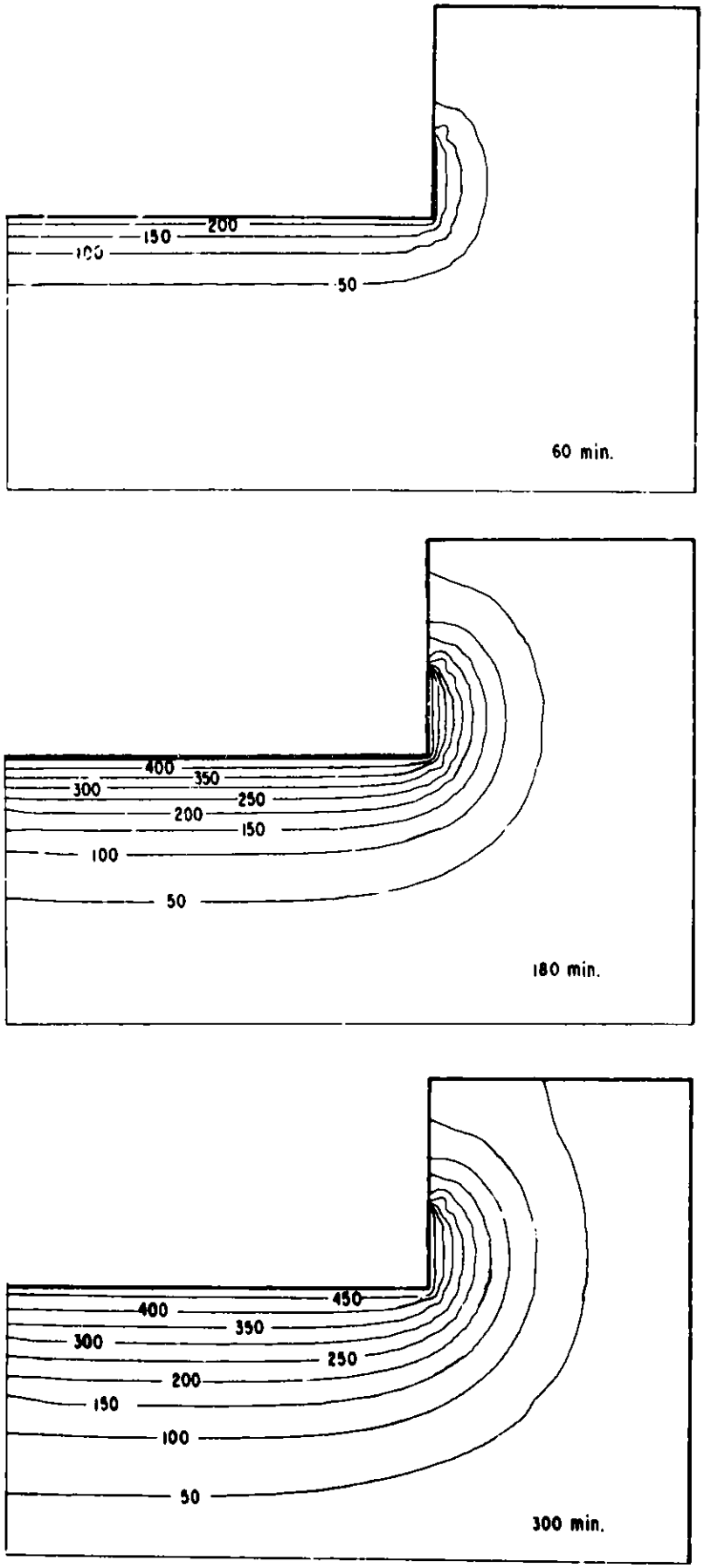

Fig. 17. Calculated Temperature Contour Plots.

use. The same temperature history is assumed for the entire wetted surface, while the remaining surface area of the crucible is taken to be ideally insulated.

2. Solution and Results

The numerical solution computes the temperature distribution from the "hot" surface through the crucible body, and yields the corresponding stress distribution within the discretized model. Sample temperature distributions at one, three and five hours from the introduction of sodium are given by the contour in Fig. 17 which compares quite well with temperatures derived using the MARK code,[5] shown in Fig. 18. The corresponding crack development due to the temperature gradients is discussed below.

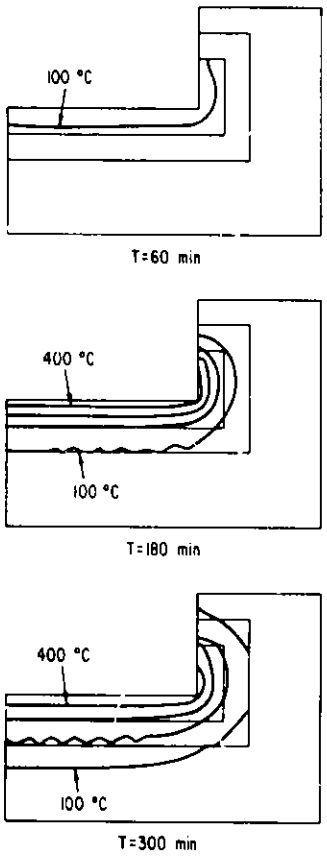

Fig. 18. Calculated Temperature Plots Using the MARC Code. (Courtesy of SANDIA National Laboratories.)

The cracking history is depicted in Figs. 19 and 20. We observe the first crack appearing at about 70 min at the bottom center of the crucible; two minutes later radial cracks begin to form at the top inside corner of the wall and propagate downward, as shown by the crack patterns at 75 min and 80 min. Several minutes later radial cracks continue propagating down the cylindrical wall and new cracks are shown to have originated: conical-circumferential cracking is observed in two locations, (a) close to the inside corner of the crucible and (b) in the mid-region of the bottom slab. It is interesting that these conical-circumferential cracks initiate internally--not at the surface of the crucible. Since the temperature is uniform in the bottom slab and is

/ CONICAL-CIRCUMFERENTIAL CRACKS * RADIAL CRACKS

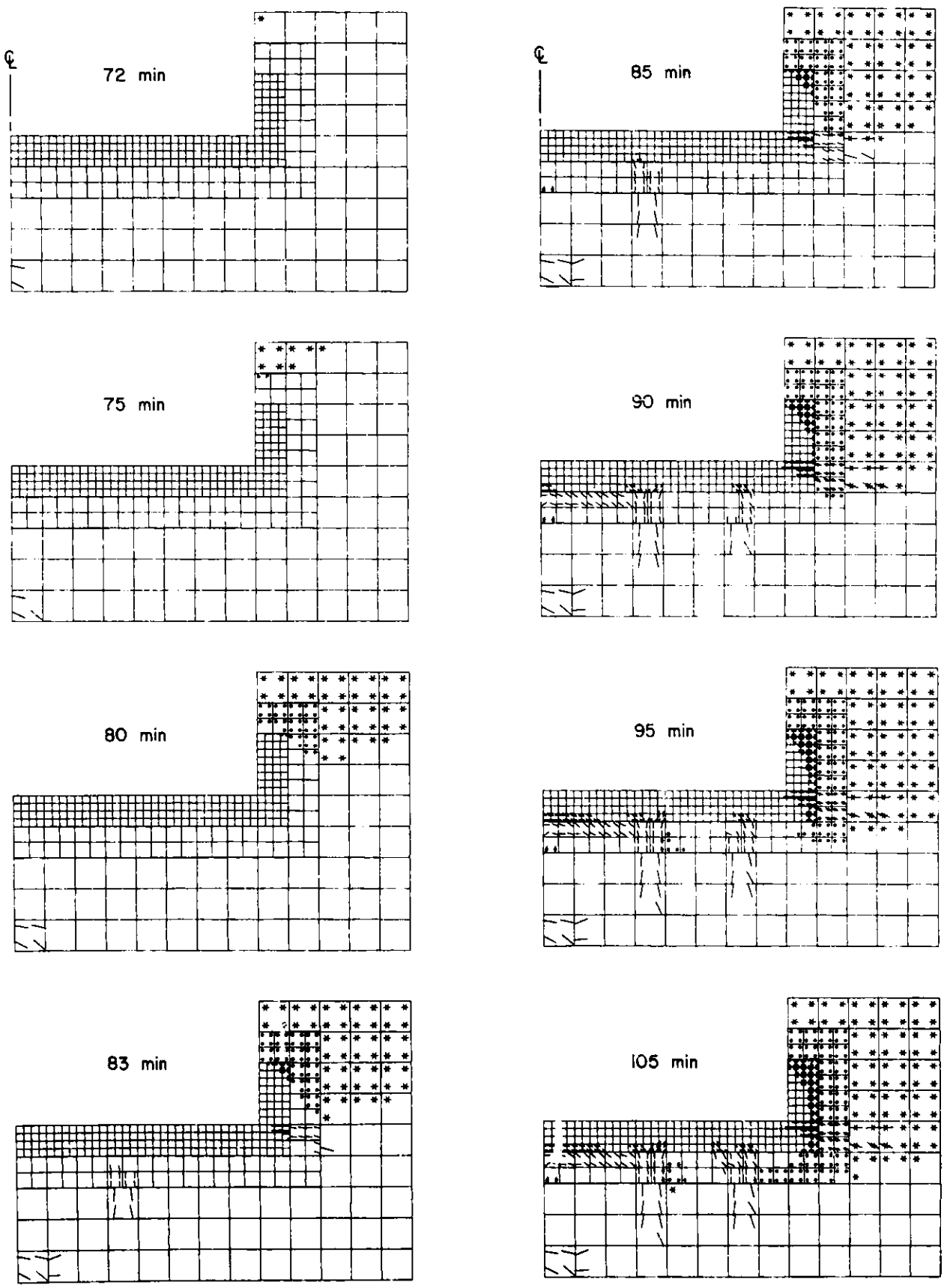

Fig. 19. Crack Distribution Patterns from 72 min through 105 min.

/ CONICAL-CIRCUMFERENTIAL CRACKS * RADIAL CRACKS

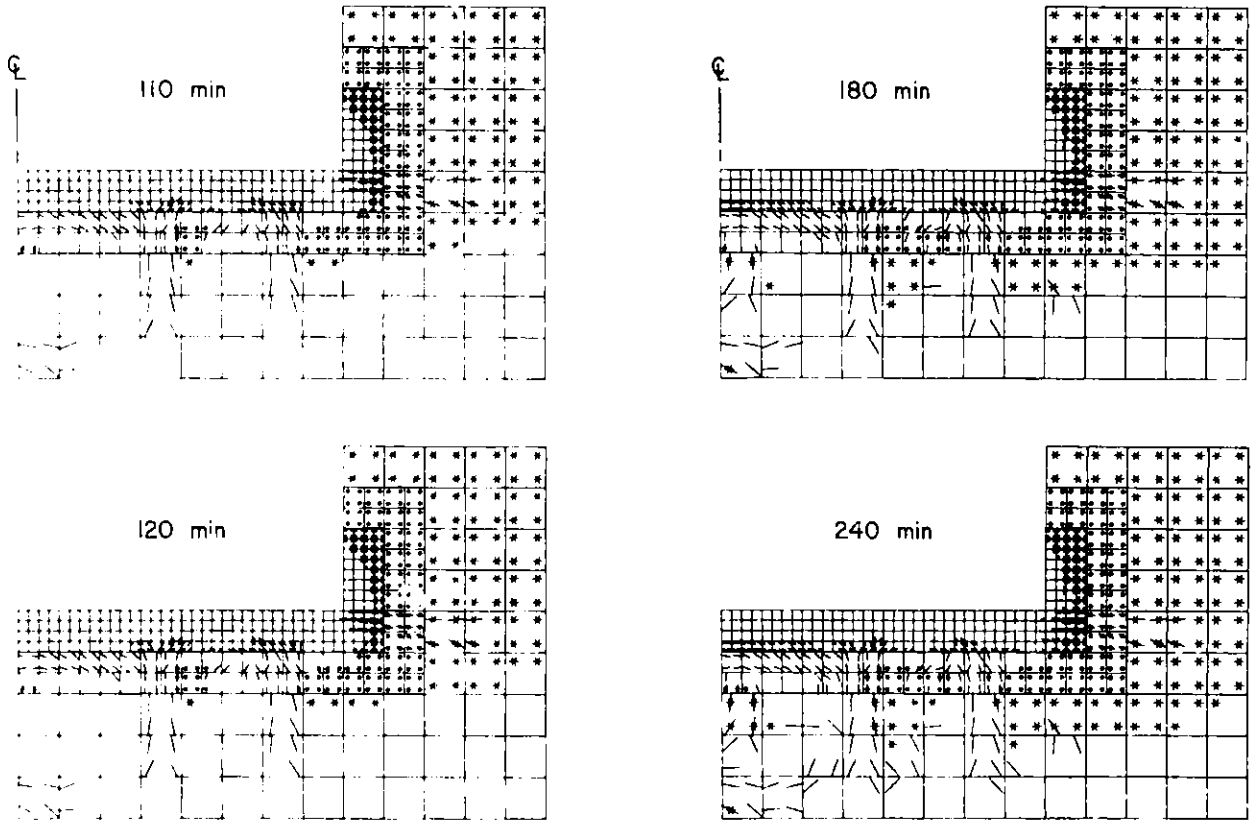

Fig. 20. Crack Distribution Patterns from 110 min through 240 min.

substantiated by the analytical model in Figs. 17 and 18, rather small temperature gradients must initiate cracking as observed in Fig. 19. The specific location in the slab at which cracks initiate thus seems to be rather arbitrary. From this time on cracks continue to form and propagate until they join other cracks. This cracking rate decreases, however, as indicated by the crack distributions at 180 and 240 min, respectively. It is also observed that in the bottom slab the cracks closest to the "hot" surface tend to be normal to the temperature gradient.

The surface cracks at 240 min correspond to the experimentally observed cracking shown in Fig. 14: complete radial cracking on the top of the cylindrical wall and partial cracking on the sides. Analysis also predicts some conical-circumferential cracks on the bottom of the crucible, but this could not be substantiated from data given in Ref. [4].

Although some steel reinforcement was used in the experiment,[5] it was not taken into account here. The effect of the reinforcement was considered showing that reinforcement attributed little to the external cracking pattern.

VII. CONCLUSIO.

Lumped mass-capacitance calculations coupled with explicit integration provide a very convenient way of calculating thermal stress. The provision of dynamic relaxation and damping make the technique quite efficient not only for transient but also for steady state problems. Computations are also economical, because the thermal part consumes only about 11% of the total time. This figure is based on four integrations per element for structural calculations and one integration per element for conductance calculations. We found one integration per element to be sufficient in the thermal calculations; all the examples given in this report are based on one integraton per element. For reference, however, if the same number of integrations is used in thermal and structural calculations, then the thermal part of the calculations would take about 30% of the total time. It should be noted that these numbers depend also on the constitutive algorithm used in the structural computations. The crucible calculations contained in this report were used to derive the figures quoted here. These coupled thermo-structural problem ran at about 3×10^{-5} seconds per element per time step. Accuracy of the thermal solutions is also quite satisfactory. Although some questions as to the effect of modeling variables still remain, we feel confident that these can be resolved without much difficulty.

We would like to stress that accuracy of our structural results should not be the main point of this illustration. The analytical cracking model used has several drawbacks which need to be improved. Rather, the capability and versatility of the coupled thermo-structural code used as an analytical tool needs to be emphasized. Even these results, however, reveal several points which should be mentioned.

One important observation of the crucible analysis is the very close proximity of cracks to the "hot" surface. With the erosion of the surface in sodium-concrete interactions these cracks would provide pathways for sodium penetration. Under these conditions deterioration of concrete could continue until all of the sodium would be consumed by the reaction.

Another feature that would enhance sodium-concrete interaction is the phenomenon, called spalling, where layers of the concrete surface peel off when subjected to intense heating. Spalling of the concrete would provide added concrete surface for sodium to react with. An indication of such spalling is the presence of cracks close and parallel to the "hot" surface. Although spalling is undoubtedly a very complex phenomenon, thermal stress may well be one of the more important contributors causing it.

With the objective of better understanding of concrete behavior under high temperature and ultimately under sodium-concrete reaction, we plan to incorporate other relevent variables into our models. Some of those considered are creep, a provision for moisture transport and pore pressure, just to name a few. Since the architecture of the code is rather simple, the incorporation of other relevant parameters should not be too difficult. The formulation based on the explicit time integration, therefore, is promising in further investigations of concrete structures under high temperatures.

Acknowledgements

Acknowledgement is extended to Dr. J. M. Kennedy for his encouragement and always ready assistance regarding the work described in this report. Appreciated is also the help provided by Dr. D. F. Schoeberle dealing with thermal problems encountered.

This work was performed under the auspices of the U.S. Department of Energy.

References

1. D. F. Schoeberle and H. L. Schreyer, personal communication.

2. C. S. Desai, "Elementary Finite Element Method," p. 307, Prentice Hall Publishers, 1979.

3. T. J. R. Hughes, K. S. Pister, and R. L. Taylor, "Implicit-Explicit Finite Elements in Nonlinear Transient Analysis," Comp. Meth. Appl. Mech. Eng., 17/18, 159 (1979).

4. Advanced Reactor Safety Report Quarterly Report July-September 1978, SAND 78-2002, NUREG/CR-0470, p. 147 (September 1979).

5. D. Swenson, SANDIA National Laboratory, personal communication.

6. G. N. Freskakis, R. C. Burros and E. B. Debbas, "Strength Properties of Concrete at Elevated Temperatures," 2nd Conf. on Civil Eng. and Nucl. Power, ASCE Structural Div., Vol. 1, Knoxville, TN, Sept. 15-17, 1980.

7. A. H. Marchertas and T. B. Belytschko. "Transient Analysis of a PCRV for LMFBR Primary Containment," Nucl. Technol., 51(3), 433-442 (1980).

8. A. H. Marchertas et al., "Analysis and Application of Prestressed Concrete Reactor Vessels for LMFBR Containment," Nucl. Eng. Design, 49 (1&2), 155-173 (1978).